Desalination and Water Treatment
www.deswater.com

doi: 10.5004/dwt.2023.29709

299 (2023) 154–171
July

Study of fractional crystallization during isothermal evaporation of Algerian inland brine at 35°C: discussion of the proposed approaches

Merzouk Zatout

Saharan Geology Laboratory, Kasdi Merbah Ouargla University, Algeria, email. zatoutm@gmail.com

Received 21 January 2023; Accepted 16 June 2023

ABSTRACT

Isothermal evaporation experiment of inland Algerian brine was carried out at 35°C. The study of fractional crystallization during this experiment has been addressed by different approaches. The identification of the solids recovered by X-ray diffraction together with the monitoring of the ionic composition, density, and pH of the evaporated brine. The Jänecke solubility diagram of the quinary system determined both predicted and experimental fractional crystallization pathways. The mass balance of $CaSO_4$, NaCl, $MgSO_4$, and KCl salts was calculated using the Zayani formulates. Finally, PHREEQC forward and inverse modeling has been done with the Pitzer thermodynamic database. The real crystallization sequences obtained are successively: gypsum and halite, halite and schoenite, halite, epsomite and sylvite, and finally halite, epsomite, sylvite, and carnallite. These results corroborate well with those obtained by both forward and inverse PHREEQC modeling but did not agree with those of Jänecke solubility diagram of the studied system at 35°C. This deviation is explained by the metastable equilibria occurred in the late stages of evaporation. Thus, PHREEQC software seems to be better when studying the evaporation of such concentrated inland brines. The calculated mass balance confirmed the possibility of the production of potassium and magnesium salts from these brines.

Keywords: Inland brine; Fractional crystallization; PHREEQC; Schoenite; Quinary diagram; Isothermal evaporation

1. Introduction

Ephemeral saline lakes of North Africa, called chotts contain supersaturated brines with total dissolved solids (TDS) up to 398 g·L^{-1} [1]. Main of these brines are Na–Mg–Cl and Na–Mg–SO_4 types [1]. The measured TDS values of brines from Algeria grade up to 398 g·L^{-1}. The salinity of brines is variable: those of the biggest chotts of Merouane and Melghir vary from 27–398 and 53–375 g·L^{-1}, respectively. The small chotts brines of Ngoussa, Safioune and Aïn Beïda show values of TDS of 224, 193 and 148 g·L^{-1}. The continental terminal groundwaters are brackish with TDS between 7 and 14 g·L^{-1} [1]. The pH value of these brines varies from 5.9 to 8.6. Their hydrochemistry is in most case Cl–SO_4/Na–Mg type except those of groundwaters (CT) and some locations with Mg > Na and SO_4 > Cl. The major ions are characterized by having Na > Mg > Ca > K, with equivalent proportions of Cl:Na, SO_4:Ca, SO_4:Mg [1]. Cl^- represents a major part of the saline content and near equivalent proportions of chlorine and sodium is 0.80, while the ratio between magnesium and sulfate is 2.5. The composition and hydrochemistry of these continental brines derive primarily from salt dissolution of the predominant lithologies across the watersheds, which consist exclusively of sedimentary rocks including anhydrite, gypsum, carbonate, and phosphate rocks. These deposits contain the terminal complex aquifer, which involves the waters of the aquifer in the primary ion supply processes. Ionic ratios and strontium isotope data reported in this aquifer by previous studies have also highlighted the presence of salt recycling, including halite,

gypsum and calcite ($CaCO_3$) [2]. This evidence supports the role of salt recycling as important sources of major solutes. The Egypt Qarun lake [3] and most of the Tunisian Chotts and Sabkha's [4] brines are characterized by the same hydrochemical facies with Na–Mg–K–Cl–SO_4. The typical ionic composition of the principal Algerian continental brines and the marine brine is plotted in Table 1. It shows that all Algerian brines are calcium and bicarbonate rich comparatively to marine brine and that of Merouane Chott is very magnesium and sulfate-rich than that marine brine. Chlorine has the same concentration for both Algerian and marine brines. Same for sodium except for Merouane Chott with lower concentration. Major ions ratios show clearly similarities between Algerian inland brines and marine brines. The exception is the Mg/Ca ratio, which is greater for marine brines. It should be noticed that Baghdad brine is the closest to the marine brine, flowed by that of Melghir. Relative to the marine brine, the most significant differences in ionic concentrations are those of Merouane brine.

The evaporation of natural water is the loss of water under the effect of heat (solar or artificial) accompanied by the precipitation of salts depending on their solubility. Many quantitative works have been realized about the evaporation of freshwater and seawater, which became a well-understood process.

The Penman–Monteith evaporation rate expression for the open water [7] given in the formula (PM equation) shows that evaporation depend on two basic factors. The first factor is the radiation factor (R_n–G), which represents the necessaire energy or heat required to transform water from liquid to vapor, and the second factor ($u_{2m}(e_s–e_a)$), which represents mechanisms involved to remove the vapor from the open water surface boundary. Therefore, there must be a sink for vapor. The Δ and γ terms in the Penman–Monteith equation translate the relationship between air temperature and vapor pressure gradients. The (1 + $0.34u_{2m}$) term reflects the combined influence of bulk and aerodynamic resistance terms for the reference open water cover.

$$\mathrm{ET} = \frac{0.408\Delta\left(R_n - G\right)}{\Delta + \gamma\left(1 + 0.34u_{2m}\right)} + \frac{\gamma\left(\frac{900}{T+273}\right)u_{2m}\left(e_s - e_a\right)}{\Delta + \gamma\left(1 + 0.34u_{2m}\right)} \quad \text{(PM equation)} \tag{1}$$

where ET: evapotranspiration rate in mm/d; (R_n–G): energy provided by radiation, which depends on approximate balance downwelling radiation (sunlight) and upwelling radiation emitted by the Earth's surface; $u_{2m}(e_s–e_a)$: potential vertical moisture flux produced by atmospheric mixing in the planetary boundary layer. u_{2m} is the wind speed and (e_s–e_a) is the vapor pressure deficit (VPD) directly linked with relative humidity. Indeed, when e_a equals 0, the air will have a relative humidity of zero. When $e_s = e_a$, the air is fully saturated, and the relative humidity will be 100%. e_a: water vapor pressure (Pa); e_s: saturation water vapor pressure (Pa); Δ: saturation water vapor curve or the first derivative of the saturated vapor pressure (e_s) with respect to air temperature near the open water surface; γ: psychrometric constant in kPa/°C, which characterizes the relation between the sensible heat and water vapor.

According to this equation, the environmental factors controlling the evapotranspiration rate are latitude, altitude, wind speed, month of the year, the reflection coefficient, minimum and maximum temperatures (°C), solar radiation ($W·m^{-2}$), and average relative humidity (%). Rate of evaporation increases proportionally with temperature, VPD, and wind velocity. It decreases proportionally with saturation water vapor and psychrometric constant.

The evaporation of open highly concentrated brines is more complex because its rate slows with the increase of TDS. Some factors such as the appearance of salt crust on the surface of brine stops the evaporation process [6]. At some extremely high-salinity, evaporation stops because the brine becomes hygroscopic and adsorbs humidity from the air rather than drying [8].

The effect of the salinity and the ionic composition on evaporation has been well studied and it is expressed by

Table 1
Typical ionic composition of the Algerian brines [5] and the typical marine brine [6]

Brine source	Chott Baghdad	Chott Merouane	Chott Melghir	Typical marine brine
Density	1.20	1.3	1.22	1.22
Total dissolved solids	345	373	345	334
Ca^{2+}	29	33	33	6
Mg^{2+}	713	2,634	1,070	971
Na^{+}	4,286	1,307	3,746	4,371
K^{+}	163	301	130	153
HCO_3^{-}	3	8	5	0
SO_4^{2-}	313	713	333	339
Cl^{-}	5,400	5,560	5,500	5,994
Cl^{-}/Na^{+}	1.25	4.3	1.46	1.37
Mg^{2+}/Ca^{2+}	23.83	79	32.18	145.4
Cl^{-}/SO_4^{2-}	17.21	7.8	16.48	17.68
Na^{+}/K^{+}	26.14	4.3	28.72	28.57
Mg^{2+}/K^{+}	4.35	8.8	8.20	6.34
Ca^{2+}/K^{+}	0.18	0.1	0.25	0.04

two principal parameters namely activity coefficient of water and the saturation vapor pressure [9]. Varieties of geochemical models exist for the determination of these parameters. The most widely used are those of the Pitzer model and the specific interaction theory (SIT) model. Pitzer's model takes into account all the interactions between all the ions present in the solution. Thus, it is considered the best model for concentrated solutions up to brines [10,11]. The weakness of this model is its over-parameterization and the lack of parameters for many elements [12], notably the silica that is always present in the system. The SIT model based on the theory that the only significant interactions are those between opposite ions. The two models are equivalent for solutions between 3 and 4 M.

During the evaporation of a brine, the loss of water in the form of vapor leads to an increase in its density [13]. This is often used as a rank parameter of the degree of evaporation of the brines. The other physico-chemical parameters which trace the evolution of evaporation are the ionic strength and the electrical conductivity which depend on the concentration of the ions present in the system [14]. During evaporation, this concentration depends on the precipitated salts according to their solubility's and the initial chemical composition of the brine. It is known that carbonates precipitate first, followed by sulfates and finally chlorides [15].

The studied brine is this work is from the closed basin Chott Baghdad situated in northeast Algeria (32°41′16.00″N, 5°37′40.00″E). Its surface is about 50 km^2 and its elevation is about 88 m above sea level. The climate is arid [16] and characterized by a mean annual temperature of 24°C, a mean annual rainfall of 6.3 mm, a mean annual evaporation greater than of 3,613 mm/month, and a mean annual humidity of 42% [17]. This chott is enclosed by Mio-Pliocene and Quaternary rocks [18]. Mio-Pliocene rocks consist of argillaceous sands, gypsum deposits, and dolomite. The Quaternary deposits are formed by sands, clays, and halite [18]. The aim of this study is to characterize and evaluate the sampled brine, in particular, from a mining point of view by carrying out an isothermal evaporation of this brine at 35°C. Indeed, the arid conditions of southeastern Algeria and particularly of Chott Baghdad favor evaporation processes. The choice of 35°C corresponds to the average temperature during the hot season (April to September) when significant changes occur in the chemistry of the brine until it dries.

This study follows two recent others [19,20] treating brines from Chott Baghdad. The spatial variation of the brine ionic composition and the good results obtained by these anterior investigations, especially the amounts of the double sulfate potassium and magnesium, and the sylvite, led to more investigation to understand and test the possibility of industrial exploitation. The chemical spatial variation has been studied [16], and the results obtained indicate that the northern part of the chott brine contains less magnesium and potassium than the southern part [16].

The main objectives of this work are: (1) determine the actual crystallization salts sequences during the isothermal evaporation experiment at 35°C by characterizing the recovered solids using X-diffraction (XRD), (2) study the brine ionic composition evolution as well as remaining volume and density, (3) calculate mass balances of the precipitated salts, (4) determine the predicted and the experimental crystallization pathways given by the Jänecke solubility diagram, (5) perform the direct and inverse modeling of the addressed isothermal evaporation experiment using the PHREEQC software; and finally (6) compare and discuss the different results.

2. Material and methods

2.1. Isotherm evaporation

The studied brine is sampled in February 2017 from subsurface natural brines ponding in the eastern side of Chott Baghdad. The density of the brine is 1.221, the pH measured in situ is 6.95 and the ionic composition measured in g·L^{-1} before starting isothermal evaporation is: Na^+ = 93.83, K^+ = 10.90, Ca^{2+} = 1.60, Mg^{2+} = 16.29, Cl^- = 180.70, SO_4^2 = 30.08, HCO_3^- = 0.19.

Four (4) liters of the above brine were placed in a crystallizer placed and fixed in a water bath filled with hot water. A thermostat was immersed in the water bath to adjust and maintain the temperature at 35°C ± 0.1°C. Isothermal evaporation was observed by daily measurements of density and pH. During evaporation, six (6) filtrations of the whole brine (with precipitated salts) were carried out with each increase of density of about one hundredth (0.01). The filtration concerns all the contents of the crystallizer, remaining brine and solids formed. The purpose of filtration is to separate the liquid phase from the solid phase. The liquid phase continued isotherm evaporation and the solid phase removed for characterization with the X-ray diffraction. Thereby, at each filtration, 20 mL sample of filtrate (the filtrates were designated Bi, i = 1 to 16) was taken to chemical analysis while the solids (the solids were designated Si, i = 1 to 6), separated by filtration, are recovered and removed from the evaporated brine. Density was carried out by using a specific gravity balance (precision of 10^{-4} g). Na^+ and K^+ concentrations were analyzed by spectrophotometer using a Jenway PFP7 Instrument (Dunmow, Essex, England). Mg^{2+} and Ca^{+2} concentrations were determined by an ethylenediaminetetraacetic acid (EDTA) complexometric titration. Potentiometric titration was applied to Cl^- (Titrino DMS 716, Metrohm Instrument, Ionenstrasse 9100 Herisau, Switzerland). The SO_4^{2-} concentrations were determined gravimetrically with barium chloride. The CO_3^{2-} and HCO_3^- concentrations were titrated with a 0.02-molar chloric acid solution using methyl-orange and phenolphthalein, respectively, as end-point indicators. XRD was used to characterize the solid phases, using a Philips PW 1730/10 Generator (Netherlands), a PW 1050/81 Goniometer and a PW 2233/20 copper cathode. The experimental work was carried out at the Saharan Geology Laboratory in February 2017 were the conditions of the experimentation are mean relative humidity of 68% and mean temperature of 10°C.

2.2. Application of the Jänecke solubility diagram approach

The quinary diagram Na^+, K^+, Mg^{2+}, Cl^-, SO_4^{2-}//H_2O, at 35°C system was studied by van't Hoff at different temperatures between 25°C and 83°C. Different geometric representations have been proposed for this system [21]. That of Jänecke corresponds to the central projection on an equilateral triangle, of the volume enveloping the solutions

saturated with halite [22]. As a result, a precipitation domain of a given salt corresponds to two solid phases, one of which is necessarily formed of halite [21]. This is the diagram adopted in this study because it is reliable, powerful, simple and comprehensible. Effectively, the initial position of the studied brine suffices to determine its crystallization field and its theoretical crystallization pathway during its isothermal evaporation [21]. Furthermore, at the end of evaporation the projection of different solutions evolved during evaporation determines the experimental pathway [22]. The theoretical pathway of the studied brine plotted on the oceanic fivefold diagram Na^+, K^+, Mg^{2+}, Cl^-, $SO_4^{2-}//H_2O$ at 35°C is based on Gibbs law:

$$v = c - \Phi \tag{2}$$

where v = system variance, Φ = phase number, and c = independents constituents' number = 5 (Na, K, Mg, Cl, SO_4).

Such as in oceanic quinary system, all the solutions are permanently saturated with NaCl. So, when a representative point is situated on a given plan (crystallization field), that means $v = 2 = 5 - \Phi$; thus, $\Phi = 3$, Two salts (halite and salt-field) and one solution. When a representative point is situated on the invariant's points, that means $v = 1 = 5 - 4$, $\Phi = 4$, three salts and one solution. At Z drying-up point, the crystallization process terminates and the solution does not move and will carry on the evaporation until drying [23].

The application of the Jänecke diagram to the studied brine presumed that calcium and carbonates are negligible constituents. This assumption is credible because of its low concentrations [3] and no back reactions of Ca-bearing minerals such as gypsum ($CaSO_4{\cdot}2H_2O$) with the brines are expected because Ca-bearing solid phases are removed from the solution at earlier stages of evaporation (2nd filtration).

The solid phases associated with halite (NaCl) of the Jänecke diagram system Na^+, K^+, Mg^{2+}, Cl^-, $SO_4^{2-}//H_2O$, at 35°C, are [21]: sylvite (KCl), hexahydrite ($MgSO_4{\cdot}6H_2O$), kieserite ($MgSO_4{\cdot}H_2O$), glaserite ($K_3Na(SO_4)_2$), thenardite (Na_2SO_4), bloedite ($Na_2Mg(SO_4)_2{\cdot}4H_2O$), kainite ($KmgClSO_4{\cdot}11/4H_2O$), leonite ($K_2Mg(SO_4)_2{\cdot}4H_2O$), bischofite ($MgCl_2{\cdot}6H_2O$), and carnallite ($KMgCl_3{\cdot}6H_2O$).

Better understand the precipitation sequences of salts during solar evaporation at 35°C of Algerian natural brine, a simulated pathway representing the evolution of the evaporated brine's composition during evaporation, given by the projection of the PHREEQC forward modeling results, was also plotted together with the two Jänecke crystallization pathways.

The Jänecke coordinates of the crystallization pathways on the Na^+, K^+, Mg^{2+}, Cl^-, $SO_4^{2-}//H_2O$, at 35°C were calculated using the following equations [21]:

$$\%K_2 = \frac{\left(n_{K^+}/2\right)\times 100}{\left(n_{K^+}/2\right)+n_{Mg^{2+}}+n_{SO_4^{2-}}};$$

$$\%Mg = \frac{\left(n_{Mg^{2+}}\right)\times 100}{\left(n_{K^+}/2\right)+n_{Mg^{2+}}+n_{SO_4^{2-}}};$$

$$\%Mg = \frac{\left(n_{Mg^{2+}}\right)\times 100}{\left(n_{K^+}/2\right)+n_{Mg^{2+}}+n_{SO_4^{2-}}} \tag{3}$$

where "n" is the mole number.

Nevertheless, many discrepancies have been reported between theoretical and experimental crystallization paths predicted using solubility diagrams at advanced stages of evaporation [20,23–27]. In addition, other discrepancies recorded between these and the crystallization path obtained from the salts recovered from elsewhere [25,26]. The state of supersaturation of the brines during the advanced stages of evaporation and the conditions of the experiment, in particular humidity and aeration, are the main causes of these deviations [26,28]. The other deviations are due to crystal nucleation, crystallization kinetics and the formation of the magnesium complex ion surrounded by six water molecules [4,20,26,29,30].

2.3. PHREEQC forward and inverse modeling with Pitzer thermodynamic database

PHREEQC is a publicly available and expandable geochemical modeling code with several thermodynamic databases based on different chemical theories. PHREEQC is widely used to simulate evaporation of natural waters because of its capability of removing moles of water from the solution [31]. In addition, the capabilities of PHREEQC include simulating the chemical behavior of aqueous solutions composed of all major solutes.

PHREEQC program provides two approaches: forward modeling and inverse modeling [32]. The evaporation forward modeling is performed by removing water from the chemical system [33] where the brine ionic composition is calculated together with water removal due to evaporation and the precipitated solid phases during evaporation [33]. Forward modelling predicts the evolution of water composition based on hypothetical reactions as crystallization or dissolution of salts during evaporation.

Along the flow path in an aquatic system, PHREEQC inverse geochemical modelling is based on a geochemical molar equilibrium model, which calculates phase molar transfers to account for differences in the final and initial composition of water [34]. Thus, the inverse modeling allows the determination of reactions from measured and observed data. Applied to the isothermal brine evaporation undertaken, the mass balance model determines the brine chemical composition and the different possible reactions between the initial and final stages. In this study, PHREEQC simulates mineral precipitation and the corresponding geochemical evolution of residual water during brine evaporation using a Pitzer database, which allows calculation of geochemical reactions in high ionic strength brines [10,33,35]. Thus, the inverse modeling allows following the ionic composition of the studied brine and the progressive crystallization sequences during its isothermal evaporation. In addition, it would fill the gap of the PHREEQC forward modeling which does not consider the mineral fractionation, for example, ions of precipitates salt are no removed from solution [28].

In the experiment studied, calcium and bicarbonate are present in relatively very low concentrations. The calcium salt was removed in the early stages of evaporation as gypsum, and the bicarbonate was below the detection limit after the first filtration. Therefore, these ions were not used

as input parameters in the PHREEQC code, as was done for the application of the Jänecke diagram. Forward modeling evaporation of black seawater has been addressed by Parkhurst and Appelo [33] to check the black seawater evaporation experiments realized by McCaffrey et al. [14]; Zherebtsova and Volkova [36]. At each water amount decrement, PHREEQC forward modeling returns water remained in a negative log of moles, ionic composition in log moles per kg of water, and mass of precipitated salts in log mole. Ion molar transfer results are expressed in moles per kg of water. Positive mass transfer values suggest the dissolution of minerals while negative values indicate precipitation. To perform inverse modeling, the inputs are the temperature, the pH, and the measured final and initial brine's ionic composition between two successive filtrations. The outputs consist of one or several models of crystallized salts and their amounts during the corresponding period (between two consecutive filtrations) in moles.

For data entry into PHREEQC, the identifiers in the inverse modeling data block were used for the selection of brine solutions; the reactive phases include halite, epsomite, schoenite, sylvite and carnallite. These phases correspond to those identified by XRD of the recovered solids (S1 to S6) during the experiment. For each simulation of two successive filtrations, the output of the run returned one or more models giving their respective solution fractions and the molar transfer of the phases. Otherwise, the sign of the Saturation Index (SI) indicates the saturation state of the brine with respect to the mineral salts. Positive SI translates the considered mineral crystallization while negative SI means its undersaturation of dissolution.

3. Results

3.1. Isotherm evaporation results

3.1.1. Physico-chemical parameters evolution

The results of the isotherm evaporation, namely, time, density, pH, remaining volume and masse of the filtrates, the masse of the solids recovered at each filtration are presented in the Table 2 together with the brine ionic composition. Density is one of the determining rank parameters used for monitoring brine evaporation [6]. In this study, it increased from 1.221 to 1.325 with different rates during evaporation (Fig. 1a). This is due to the difference of the precipitated salts. The remaining brine volume evolution was followed (Fig. 1b) and we notice that at the end of evaporation the volume of the residual brine is only 1.88% and, as like density, it decreased with different rates. The mass of the total solids recovered is 1,718 g.

During evaporation, Na^+ decreased continuously from density 1.221 to density 1.325 expressing the continuous crystallization of halite (Fig. 1c). Cl^- undergone a stationary curve until density of 1.312 at which it increased rabidly (Fig. 1d). K^+ and SO_4^{2-} increased from the beginning until density of 1.312 and then SO_4^{2-} started decreases followed immediately by the diminution of K^+ and at density 1.316 expressing the crystallization of K_2SO_4 and $MgSO_4$ (Fig. 1c and d). The simultaneous decrease of the ratios K^+/Mg^{2+} and SO_4^{2-}/Mg^{2+} (Fig. 2) confirmed this observation. These salts consist of schoenite, epsomite, sylvite, and carnallite as confirmed by X-ray diffraction (§3.1.2). Ca^{+2} disappeared completely at density 1.235 (Fig. 1d) as gypsum, which is recovered in the earlier stages of evaporation.

3.1.2. Identification of the recovered salts by X-ray diffraction

The actual crystallization sequences obtained after characterization of the recovered solids S1 to S6, by X-ray diffraction. X-ray diffraction patterns of the six solids recovered from the six filtrations presented in Fig. 2. The salts identified define five (5) crystallization sequences (Table 3).

Gypsum and sodium chloride crystallized together between densities from 1,223 to 1,235. Then, halite alone until density of 1.275. The apparition of gypsum in the first stage of evaporation corroborates well with the evaporation of seawater and inland brine as it the first mineral, which precipitates [6] and references therein. The presence of minor amounts of calcium in the initial solution, which is concentrated in sulfate ion, and with because of its very low solubility, gypsum will precipitate.

Salt-3 precipitated between densities 1.275 and 1.312 is a mixture of halite and schoenite ($K_2SO_4 \cdot MgSO_4 \cdot 6H_2O$). Salt-4 crystallized between d = 1,312 and d = 1,319 consists of halite, epsomite ($MgSO_4 \cdot 7H_2O$), and sylvite (KCl). Finally, salt-5 composed of halite, epsomite, carnallite (KCl $MgSO_4 \cdot 6H_2O$) and sylvite crystallized between densities 1.319–1.325.

The ionic composition of the recovered solids, presented in Table 4, shows that: solids 1 and 2 are mainly composed of halite and a minor amount of gypsum, particularly solid-2. Solid-3 consists of halite; solid-4 contains, in addition to halite, a double salt of magnesium and potassium sulfate with a K/Mg ratio equal to one; solid-5 contains more potassium and magnesium, reflecting the precipitation of potassium and magnesium sulfate; and finally, solid-6 contains the highest value of magnesium and sulfates. The K/Mg ratio of the last solids reflects the absence of double salts since it is different from one. These results corroborate well with those given by XRD and confirm the crystallization of salts other than halite and epsomite.

3.1.3. Saturation state of the filtrates during evaporation

Equilibrium diagrams plotted in Fig. 3 of the 17 brines sampled during evaporation during isotherm evaporation (listed in Table 2) show clearly the continuous crystallization of halite since sodium concentration decreased with the increase of chloride. Moreover, all equilibria diagrams corroborate well with the results of X-ray diffraction. Indeed, the totality of gypsum has been crystallized before the 1st filtration corresponding to sample B4-S1. Moreover, the short period of schoenite crystallization between B11 and B12-S4 is in good agreement with the solid-4 found by XRD. Then, schoenite disappeared after B13 and did not reveal by XRD in salts 5 and 6. Effectively, the equilibria of the solutions B13 to B16 are identical to those before the precipitation of the schoenite (IB to B10), while magnesium concentrations increased progressively with evaporation (Fig. 3). The equilibrium diagram of epsomite translates its precipitation from B11 until the end of evaporation that XRD confirmed. Sylvite started crystallization at B13 and was recorded by XRD of B14-S5. Finally, carnallite crystallized at B14 and was well

Table 2
Experimental results: measurements and physico-chemical analysis of the studied brine isotherm evaporation at 35°C

Time (h)	Sample code	Density	pH	RLm	RSm	Na^+	K^+	Mg^{2+}	Ca^{2+}	Cl^-	SO_4^{2-}
0	IB	1.223	6.94	4,952.1	0	93.83	10.9	16.29	1.6	180.7	30.08
	B1	1.224				92.15	11.2	18.28	1.32	184.2	33.1
	B2	1.226				87.5	12.2	20.15	1.04	184.12	35.3
	B3	1.227				83.95	13	22.15	0.76	184.52	38.22
48	B4-S1	1.235	6.85	3,020.4	607.5	78.65	15.6	24.75	0.48	184.42	42.12
	B5	1.237				72.54	18.25	27.83	0.2	184.56	47.56
	B6	1.245				64.25	21.6	33.25	0.08	184.95	54.96
120	B7-S2	1.254	6.79	1,788.5	359.7	59.95	22.2	37.19	udl	185.65	62.12
	B8	1.257				54	24.8	40.84	udl	186.05	66.14
168	B9-S3	1.275	6.73	1,270.6	178.5	50	26	48.26	udl	187.55	77.23
	B10	1.285				42	27.8	57.25	udl	195.42	90.46
	B11	1.309				34.52	34.2	70.62	udl	206.45	95.45
216	B12-S4	1.312	6.51	541.4	355.9	30	35.8	75.97	udl	221.45	88.45
	B13	1.316				23.5	33.1	82.9	udl	233.1	82.12
288	B14-S5	1.319	6.39	260	149.6	22.45	26.6	85.81	udl	245.65	74.96
	B15	1.321				18	20.12	89.52	udl	268.54	60.13
336	B16-S6	1.325	5.90	88.2	66.8	14.2	13.5	98	udl	297.12	35.6

IB is initial brine; Bi-Sj: brine *i* and salt *j* from each filtration; RLm: remaining liquid mass (g); RSm: recovered solids mass (g); ions concentrations in g·L^{-1}, udl: under detection limit. HCO_3^- and CO_3^{2-} are under limit of detection except for the initial brine with HCO_3^- equal to 0.19 g·L^{-1}.

identified by XRD of B16-S6. Thus, the equilibrium diagrams of the brine samples during the experiment confirmed well the real crystallization sequences given by XRD.

3.1.4. Material balance of the deposited salts and the evaporated water

To evaluate the mining potential of the studied brine, it is necessary to determine the quantity of each salt recovered during the isotherm evaporation. To do this, the method given by Zayani and Rokbani [37] have been applied. The first step is the determination of the crystallization stages of hypothetical salts presents in the system, namely $CaSO_4$, Na_2Cl_2, $MgSO_4$, K_2Cl_2 and $MgCl_2$. This, by calculating the concentrations of all ions in mole per 1,000 moles of water. For this purpose, it was necessary to transform the ionic composition results into hypothetical mineralogical compositions in moles per 1,000 moles of water by using the Eq. (4) given by Zayani and Rokbani [37].

$$\left(C_i\right)_j = \frac{\left(c_i\right)_j 1{,}000}{M_i\left(n_{H_2O}\right)_j} \tag{4}$$

where $(C_i)_j$ is the concentration of the *i*-th ion in the *j*-th sample, expressed in moles per 1,000 moles of water, $(c_i)_j$ the concentration in g·L^{-1} of the *i*-th ion in the *j*-th sample, M_i is the molar mass of the *i*-th ion and $\left(n_{H_2O}\right)_j$ is the number of moles of water in 1 L of the *j*-th sample.

The second step is the determination of moles of different salts as a function of the number of moles of $MgCl_2$. The number of moles of different salts $n_{(X)}$ were calculated as follows:

$$n_{(Na_2Cl_2)} = \frac{n_{Na^+}}{2} \tag{5}$$

$$n_{(MgSO_4)} = n_{\left(SO_4^{2-}\right)} - n_{(CaSO_4)} \tag{6}$$

$$n_{(K_2Cl_2)} = \frac{n_{K^+}}{2} \tag{7}$$

$$n_{(MgCl_2)} = n_{\left(Mg^{2+}\right)} - n_{(MgSO_4)} = \frac{n_{Cl^-}}{2} - n_{(Na_2Cl_2)} - n_{(K_2Cl_2)} \tag{8}$$

Table 5 presents the variations of number of moles of hypothetical salts per 1,000 moles of water, plotted in Fig. 4, which shows clearly that magnesium chloride being the most water-soluble salt. It is therefore useful to represent the evolution of the others salts as a function of that of $MgCl_2$. This representation (Fig. 4) is justified by the remark by Prigogine and Defay [38] which stipulates that the solvent H_2O cannot be assimilated to a simple continuous medium since its molecular structure undergoes alteration.

The curves in Fig. 5 indicate clearly three crystallization sequences corresponding to a succession of crystallization of NaCl, $MgSO_4$, and K_2Cl_2. Due to the low quantity of Ca^{2+} in the brine, $CaSO_4$ disappears following the sixth liquid sampling (2nd filtration) during the evaporation. Furthermore, NaCl evolves according to a decreasing curve and $MgSO_4$ together with K_2Cl_2 evolve according to maximum curves. These observations translate that NaCl crystallizes permanently during evaporation and that the salts of $MgSO_4$ and K_2Cl_2 only begin to precipitate when the concentration of $MgCl_2$ reach 40 and 48 moles/1,000 moles

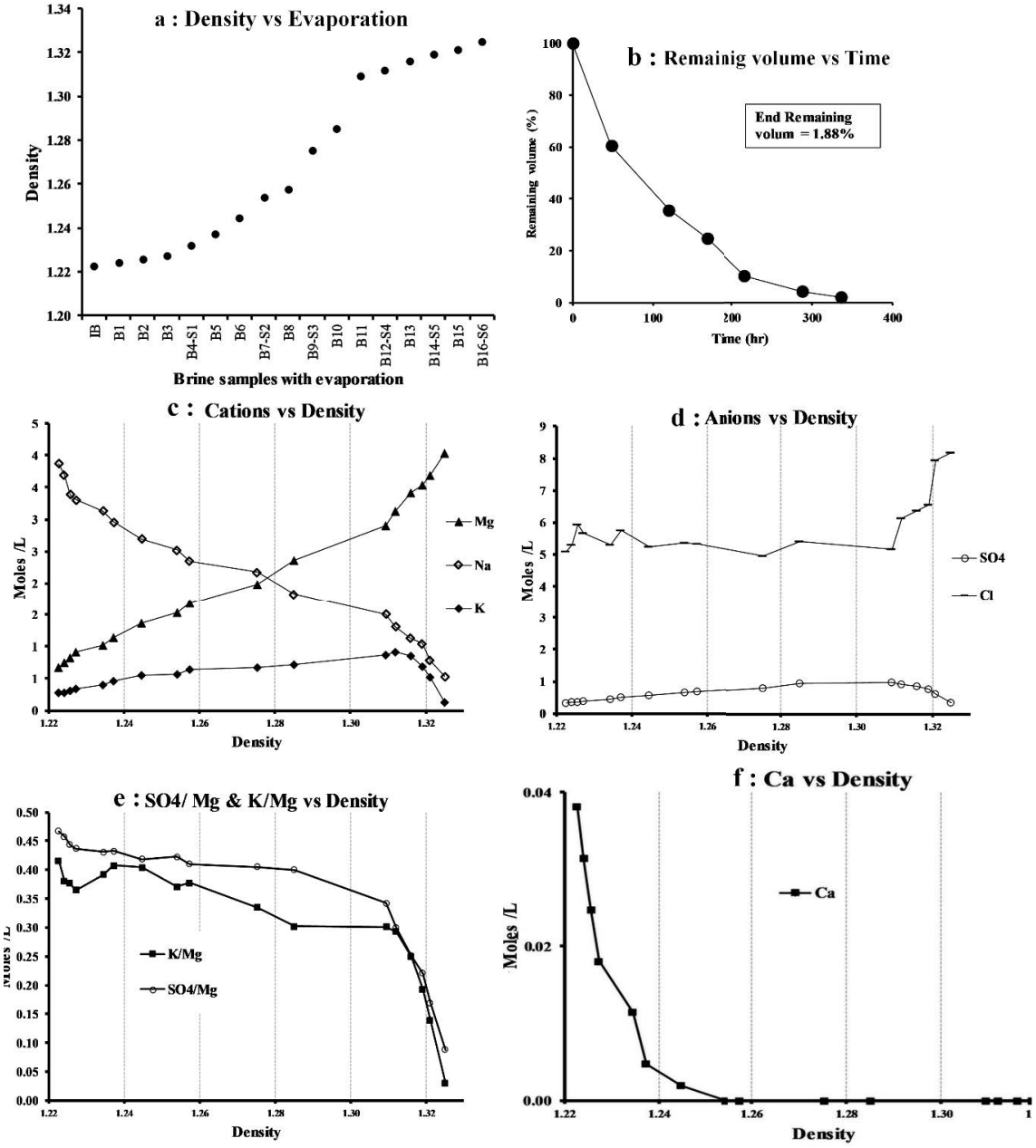

Fig. 1. Physico-chemical parameters evolution during 35°C IEE Isothermal Evaporation Experiment. (a) Density vs. evaporation, (b) remaining volume vs. time, (c) cations vs. density, (d) anions vs. density, (e) SO_4/Mg & K/Mg vs. density and (f) Ca vs. density.

of water, respectively. This may reflect that potassium and magnesium salts do not crystallize together until after the concentration $MgCl_2$ exceeds 48%.

Regarding the material balance of deposited salts and evaporated water, we assumed that the ions in solution were associated in the form of simple salts: $CaSO_4$, $MgSO_4$, K_2Cl_2 and $MgCl_2$. During evaporation, these salts crystallize successively depending on their solubility. The curves in Fig. 5 can be divided into four parts, separated by lines Ж0, Ж1, Ж2, Ж3 and Ж4. The amounts of evaporated water and crystallized salts were determinate from these parts corresponding to the following brine compositions:

Brine	Density	$MgCl_2$	Na_2Cl_2	K_2Cl_2	$MgSO_4$	$CaSO_4$	H_2O
Ж0	1.223	7.24	41.38	2.83	5.54	0.81	1000
Ж1	1.245	16.17	28.40	5.61	11.59	0.04	1000
Ж2	1.309	40.87	16.05	9.35	21.25	0.00	1000
Ж3	1.312	47.44	14.04	9.85	19.82	0.00	1000
Ж4	1.325	77.74	6.56	3.67	7.87	0.00	1000

In order to simplify the writing of the expression of the material balance, the numbers of moles of H_2O, $CaSO_4$, Na_2Cl_2, $MgSO_4$, K_2Cl_2 and $MgCl_2$ in relation to 1,000 moles

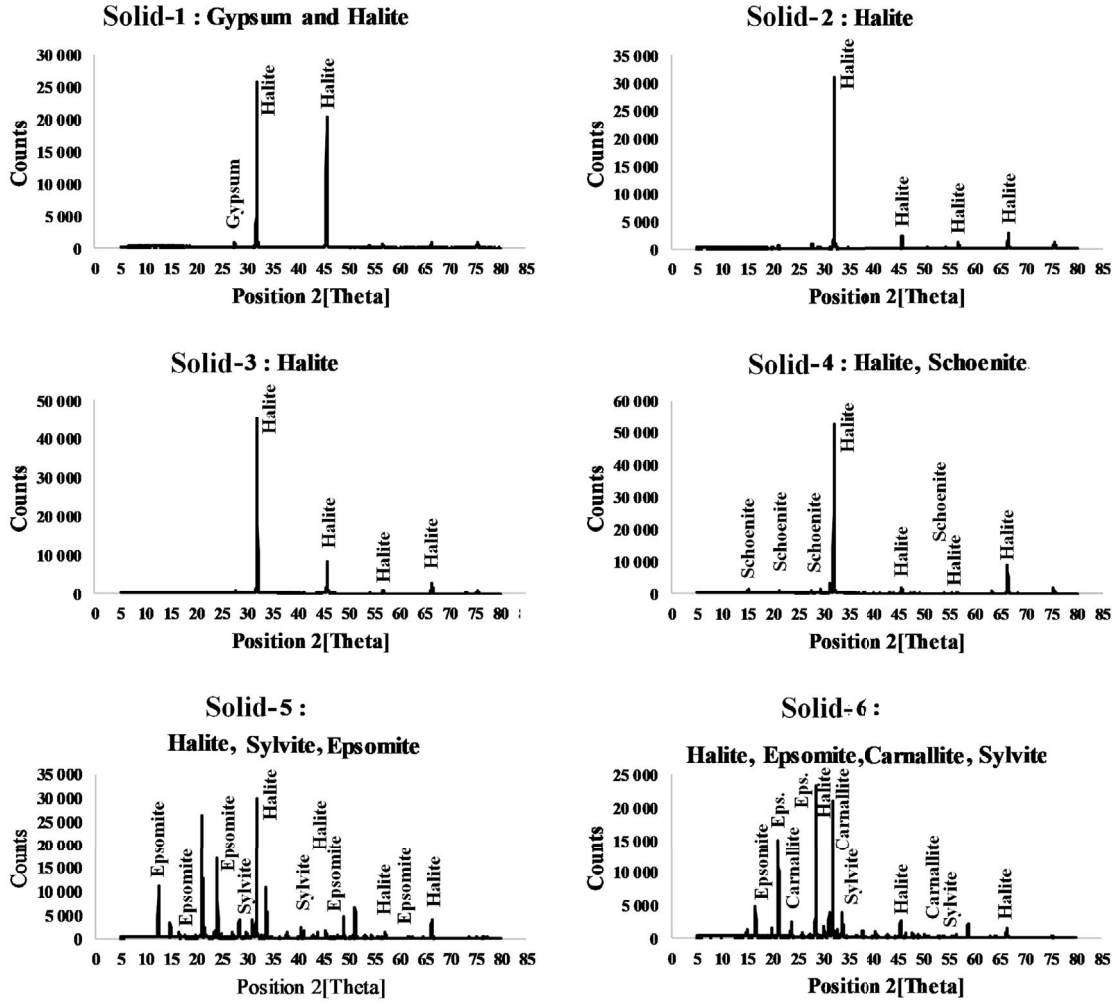

Fig. 2. X-ray diffraction patterns of the recovered solids.

Table 3
Recovered solids characterization and actual crystallization sequences

Solids (Si)	Density	Solid phase (identified by XRD)	Crystallization sequences	
			Salt number	Salts
Solid-1	1.235	Gypsum + Halite	Salt-1	Gypsum + Halite
Solid-2	1.254	Halite	Salt-2	Halite
Solid-3	1.275	Halite		
Solid-4	1.312	Halite, Schoenite	Salt-3	Halite, Schoenite
Solid-5	1.319	Halite, Epsomite, Sylvite	Salt-4	Halite, Epsomite, Sylvite
Solid-6	1.325	Halite, Epsomite, Carnallite, Sylvite	Salt-5	Halite, Epsomite, Carnallite, Sylvite

of water in the brine ⋇i are represented by H^i, C^i, N^i, M^i, K^i and Mc^i, respectively. The number of moles of water evaporated and the numbers of moles of $CaSO_4$, Na_2Cl_2, $MgSO_4$, K_2Cl_2 crystallized between ⋇i and ⋇j are given by H^{i-j}, C^{i-j}, N^{i-j}, M^{i-j} and K^{i-j}, respectively. They were calculated using Eqs. (9)–(15) given by Zayani and Rokbani [37] $MgCl_2$ does not precipitate and it conserves its mole number during evaporation.

The number of moles of water evaporated and number of moles of NaCl, N^{0-1} crystallized in the first part can be calculated by the following equation:

$$H^{0-1} = H^0\left(1-\alpha\right) \tag{9}$$

$$N^{0-1} = N^0\left(1-\alpha\right) \tag{10}$$

Table 4
Recovered solids ionic composition (%)

Solids	Density	Ca^{2+}	Mg^{2+}	Na^{+}	K^{+}	Cl^{-}	SO_4^{2-}
Solid-1	1.235	0.40	1.50	35.00	0.30	57.00	5.80
Solid-2	1.254	0.30	2.20	35.45	0.22	57.33	4.50
Solid-3	1.275		2.21	35.17	1.24	57.68	3.71
Solid-4	1.312		7.19	26.57	1.20	51.48	13.55
Solid-5	1.319		8.70	13.04	13.91	33.04	31.30
Solid-6	1.325		12.94	8.63	9.84	15.76	52.83

where $\alpha = Mc^0/Mc^1$: concentration factor of the first stage.

Analogically with the study [37], the number of moles of $CaSO_4$, C^{0-1} crystallized in the first part, can be calculated via the following equation:

$$C^{0-1} = C^0\left(1-\alpha\right) \tag{11}$$

The number of moles of water evaporated, H^{1-2}, and the number of moles of NaCl crystallized, N^{1-2}, in the second part can be calculated by using the following equations:

$$H^{1-2} = \alpha * H^0\left(1-\beta\right) \tag{12}$$

$$N^{1-2} = 2N^1\left(1-\beta\right) \tag{13}$$

where $\beta = Mc^1/Mc^2$: concentration factor of the second stage.

In the third part, the number of moles of water evaporated, H^{2-3}, and the numbers of moles of NaCl, N^{2-3}, $MgSO_4$, M^{2-3} and K_2Cl_2, K^{2-3} crystallized can be calculated by using the following equations:

$$H^{2-3} = \alpha \times \beta \times H^0\left(1-\gamma\right) \tag{14}$$

$$N^{2-3} = 2N^2\left(1-\gamma\right) \tag{15}$$

where $\gamma = Mc^2/Mc^3$: concentration factor of the third stage.

Finally, in the fourth part of Fig. 4, the number of moles of water evaporated, H^{3-4}, and the numbers of moles of NaCl, N^{3-4}, $MgSO_4$, M^{3-4} and K_2Cl_2, K^{3-4} crystallized can be calculated by using the following equations:

$$H^{3-4} = \alpha \times \beta \times \gamma \times H^0\left(1-\theta\right) \tag{16}$$

$$N^{3-4} = 2N^3\left(1-\theta\right) \tag{17}$$

$$M^{3-4} = M^3\left(1-\theta\right) \tag{18}$$

$$K^{3-4} = 2K^3\left(1-\theta\right) \tag{19}$$

where $\theta = Mc^3/Mc^4$.

For the studied Algerian brine, calculations performed for a quantity of the brine containing 1,000 moles of water are given in the Table 6. These results indicate that after evaporation 90% of water, the mass percentages of recovered salts are 71.21% of NaCl, 17.77% of $MgSO_4$ and 9.84% for KCl. Thus, more than a quarter of the salts recovered mass consists of potassium chloride and magnesium sulfate.

The total mass of solids calculated for 1,000 moles with this method is 7,683.5 g. 1,000 moles of water correspond to 18,000 g of water. This correspondent mass of solids related to the brine evaporated mass in the undertaken experiment which is 4,000 g, is = 7.683 × 4,000/18,000 = 1,707.33 g. The actual mass of solids recovered is 1,718 g. The difference is 0.6% without taking into account the masse of the water contained in the hydrated salts of picromerite, epsomite and carnallite. As given by the solubility diagram, picromerite is present in low quantities. Same for carnallite, which is in the beginning of crystallization. Contrary to epsomite, which is present in considerable quantities. Thus, the calculated balance sheet is satisfactory.

3.2. Jänecke theoretical and experimental crystallization pathway

The projection on the initial brine on the Jänecke Na^+, K^+, Mg^{2+}, Cl^-, $SO_4^{2-}//H_2O$ at 35°C phase solubility diagram in solid blue triangle (Fig. 6) gives the location of the representative point 'z' of the studied brine on the oceanic quinary diagram. It is located in the bloedite crystallization field as for of that of the seawater. Thus, the Algerian natural brine is a marine-like brine richer in potassium (Fig. 6). This position (z) together with the bloedite representative point allow plotting its theoretical crystallization pathway (Fig. 7). Consequently, the predicted theoretical Jänecke crystallization salts sequences are determined. The two superposed point's zz' translates that the brine crystallized only halite because coordinates of SO_4 and K become unchanged despite their increasing, that is, that the brine concentrating with these ions but without precipitating as salts. Therefore, the brine did not move and crystallized halite alone. Then, when it crystallized others salts than halite, it moved along the crystallization path. This, translated by the change in the K and SO_4 Jänecke coordinates. In addition, each segment corresponds to a specific association of minerals as follows:

1. zz' (v = 3): Halite
2. z'β (v = 2): Halite + Bloedite
3. βV: Halite + Bloedite + Leonite
4. VY: Halite + Bloedite + Kainite
5. Y'Y: Halite + Kainite + Hexahydrite
6. YR: Halite + Kainite + Kieserite
7. RZ: Halite + Kieserite + Carnallite

The invariable points V, Y', Y, R, defined the borders of the minerals fields. At each point, dissolution (decomposition) of previous salt and crystallization (apparition) of new salt occurred as follows:

V : Decomposition of leonite and apparition of kainite ($KMgClSO_4 \cdot 11/4H_2O$)
Y' : Dissolution of bloedite and apparition of hexahydrite ($MgSO_4 \cdot 6H_2O$)
Y : Dissolution of hexahydrite and apparition of kieserite ($MgSO_4 \cdot H_2O$)
R : Dissolution of kainite and apparition of carnallite ($KMgCl_3 \cdot 6H_2O$)
Z : The brine did not move until the complete drying

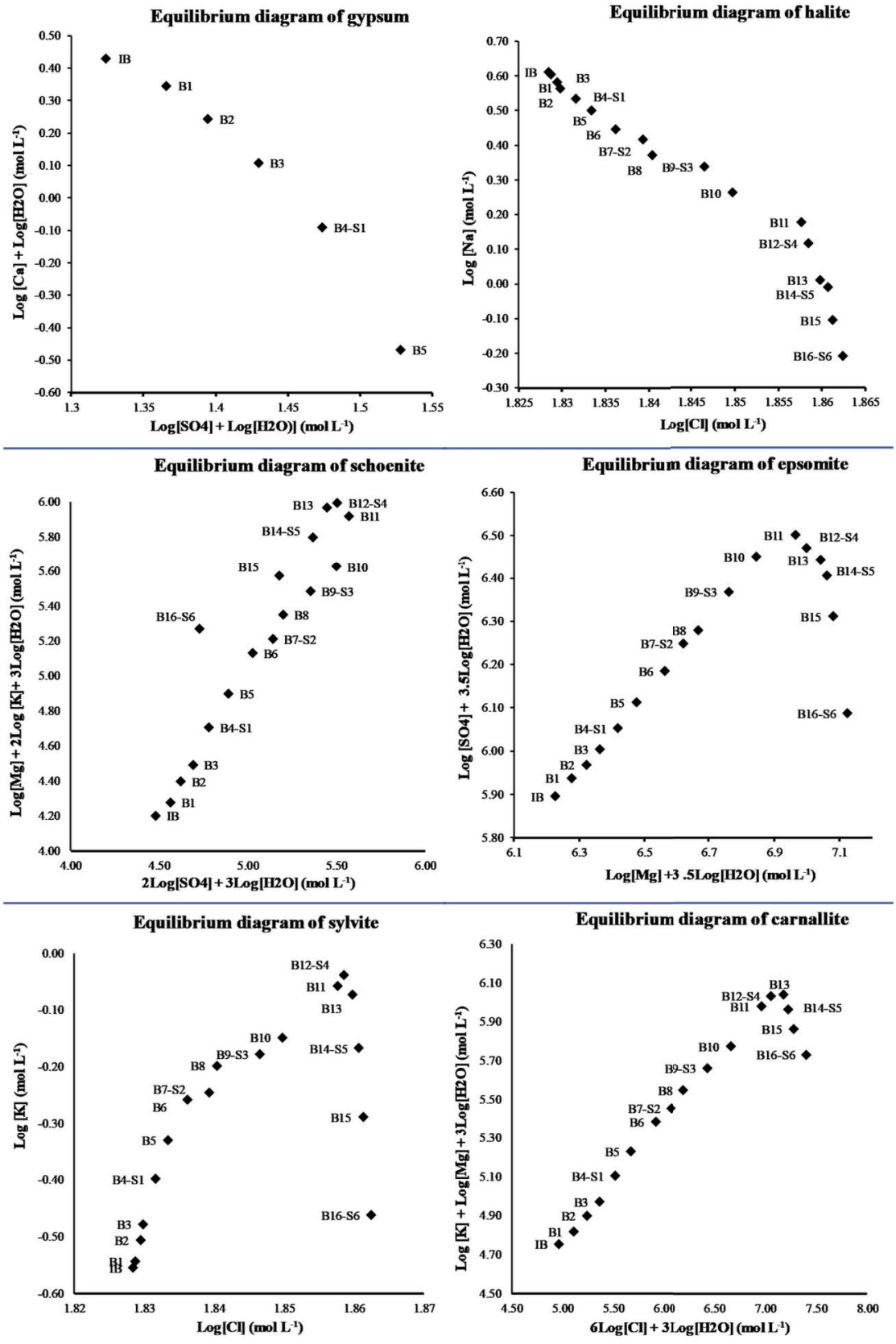

Fig. 3. Equilibrium diagrams of the sampled brines (Table 1) with respect to the recovered salts (gypsum, halite, shoenite, epsomite, sylvite, and carnallite).

Table 5
Hypothetical mineralogical compositions (concentrations in moles per 1,000 moles of water)

Brine (Bi)-Salt (i)	Density	Na_2Cl_2	K_2Cl_2	$MgSO_4$	$MgCl_2$	$CaSO_4$	H_2O
IB	1.223	41.38	2.83	5.54	7.24	0.81	1000
B1	1.224	40.82	2.92	6.34	8.30	0.67	1000
B2	1.226	38.69	3.17	6.94	9.38	0.53	1000
B3	1.227	37.15	3.38	7.71	10.44	0.39	1000
B4-S1	1.235	34.75	4.05	8.66	11.77	0.24	1000
B5	1.237	32.04	4.74	9.95	13.20	0.10	1000
B6	1.245	28.40	5.61	11.59	16.17	0.04	1000
B7-S2	1.254	26.61	5.79	13.20	18.03	0.00	1000
B8	1.257	23.87	6.45	13.99	20.15	0.00	1000
B9-S3	1.275	22.27	6.81	16.46	24.19	0.00	1000
B10	1.285	19.01	7.40	19.60	29.42	0.00	1000
B11	1.309	16.05	9.35	21.25	40.87	0.00	1000
B12-S4	1.312	14.04	9.85	19.82	47.44	0.00	1000
B13	1.316	11.00	9.11	18.40	55.00	0.00	1000
B14-S5	1.319	10.49	7.31	16.77	59.10	0.00	1000
B15	1.321	8.38	5.51	13.40	65.44	0.00	1000
B16-S6	1.325	6.56	3.67	7.87	77.74	0.00	1000

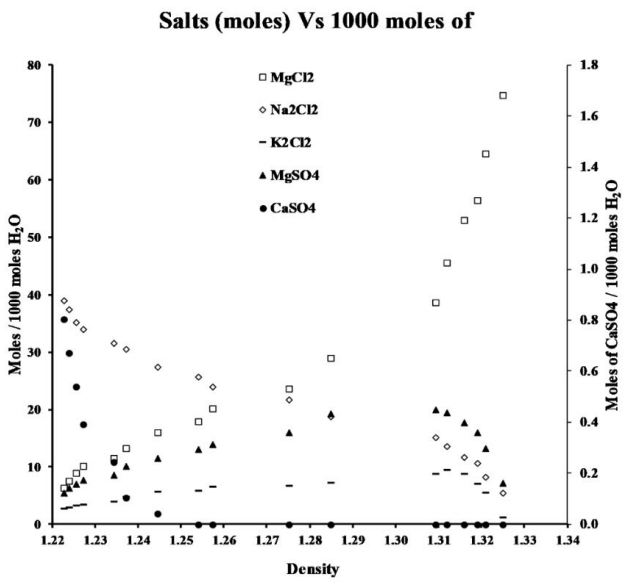

Fig. 4. Variation of moles numbers of salts as a function of density.

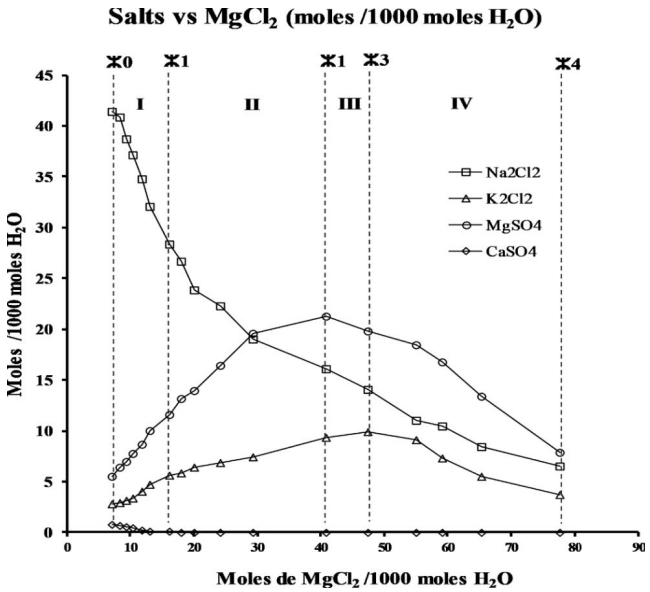

Fig. 5. Moles numbers of salts as a function of the moles number of $MgCl_2$.

The projection of initial brine (IB) and the filtrated brines (Bi, *i*: 1 to 9) plotted in Table 7 on the Jänecke Na^+, K^+, Mg^{2+}, Cl^-, $SO_4^{2-}//H_2O$ at 35°C phase solubility diagram in solid blue triangle (Fig. 7) corresponds to the Jänecke experimental crystallization pathway followed by the brine during evaporation. In the beginning of evaporation, the Jänecke coordinates did not change notably because of the precipitation of halite alone. So, the representative points of these brines are confounded. According to Fig. 7, the crystallization salts sequences given by the experimental pathway are:

1. Halite
2. Halite + Bloedite
3. Halite + Bloedite + Leonite
4. Halite + Kainite
5. Halite + Kieserite + Carnallite

The three first theoretical sequences 1–3 and the last theoretical sequence 7 are in a good agreement with those of the Jänecke experimental ones. Contrarily to the three forecast sequences 4–6, which are different to that of experimental

pathway. Indeed, the path of the experimental pathway barely touches the domain of leonite and crosses the ridge of the two fields bloedite and kainite to penetrate directly into the domain of kainite.

3.3. PHREEQC modeling results

3.3.1. PHREEQC forward modeling results

Except calcium and carbonate, all the major ions of Baghdad natural brine used as input parameters in the code.

Table 6
Material balance calculated for brine moles in 1,000 moles of water

Stages	Component				
	H_2O	$CaSO_4$	NaCl	$MgSO_4$	K_2Cl_2
First stage	822.92	0.67	68.11		
Second stage	21.12		7.86	2.94	
Third stage	36.29		12.51	8.28	7.29
Fourth stage	22.14		5.11	3.07	2.86
Evaporated water	902.47				
Numbers of moles per 1,000 moles of water		0.67	93.60	14.29	10.15
Mass percentage (%)		1.18	71.21	17.77	9.84

Thus, as for Jänecke diagram approach, the starting brine ionic composition (in $g{\cdot}L^{-1}$) introduced in PHREEQC code is $Na^+ = 93.83$, $K^+ = 10.90$, $Mg^{2+} = 16.29$, $Cl^- = 180.70$, $SO_4^{2-} = 30.08$.

Calcium and carbonate were not included because back reactions of Ca phase can occur as indicated in §2.2 (application of Jänecke quinary diagram Na^+, K^+, Mg^{2+}, Cl^-, SO_4^{2-}//

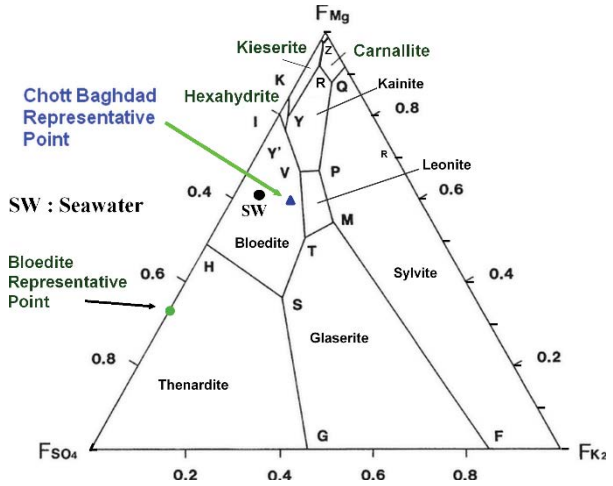

Fig. 6. Location of the representative point of the studied brine on the oceanic quinary diagram Na^+, K^+, Mg^{2+}, Cl^-, SO_4^{2-}//H_2O at 35°C.

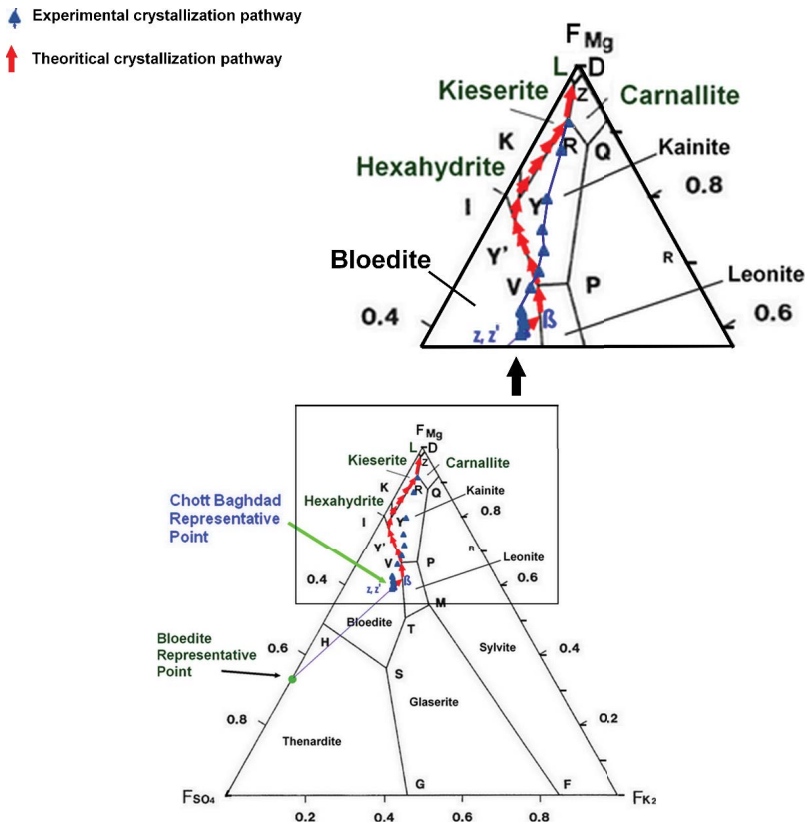

Fig. 7. Experimental and theoretical and pathways of Chott Baghdad brine on the oceanic quinary diagram Na^+, K^+, Mg^{2+}, Cl^-, SO_4^{2-}// H_2O at 35°C.

Table 7
Jänecke coordinates of solutions brines

Brine (Bi)	%Mg	%K	%SO_4
IB	59.68	12.42	27.90
B4-S1	61.47	12.05	26.49
B7-S2	62.17	11.54	26.29
B9-S3	63.58	10.65	25.76
B11	66.99	10.09	22.92
B12-S4	69.38	10.17	20.45
B13	72.73	9.03	18.24
B14-S5	75.90	7.32	16.78
B15	80.65	5.64	13.71
B16-S6	88.12	3.78	8.10

H_2O, at 35°C). Furthermore, calcium is present with very relatively low concentrations and removed from the brine as gypsum. Therefore, the precaution of starting simulation with free calcium is reliable.

The results of the forward modeling presented in Fig. 8 shows that until the degree of evaporation of 98%, the major's ion behavior agreed very well to the experimental results. Na decreased, Cl undergone a stationary behavior, K and SO_4 undergone a maximum curve evolution, and Mg increased continuously. Similarly, the salts sequences agreed very well to those obtained in the recovered solids and characterized by X-ray diffraction. These salts crystallization sequences are successively halite, halite + schoenite, halite + sylvite + epsomite, and finally, halite + epsomite + carnallite + sylvite. Thus, the forward modeling of the Algerian natural brine evaporation at 35°C gave exactly the same results obtained in the experiment. Furthermore, the projection of the degree of evaporation of the six filtrations carried out during experimental work corroborate well in term of the nature of the recovered solids. This finding establishes that forward modeling using PHREEQC with Pitzer thermodynamic database evaporation is also reliable for high-saturated brines. This result comforts the finding of when comparing the different thermodynamic databases [39]. Indeed, the Pitzer database found reliable up to six moles equivalent NaCl saturated brine, thus up to TDS of 348 g·L^{-1}.

3.3.2. PHREEQC inverse modeling results

Evaporation inverse modeling of the Algerian brine has been done using the real ionic compositions of the brine at the six filtrations presented in Table 2. Six simulations carried out between each two successive filtrations. Between solutions S1 and S5, S5 and S8, S8 and S10, S10 and S13, S13 and S15, and finally between S15 and S17. The results of the inverse modeling presented in Table 8. The program returned one model for each of the four first simulations, which consist of gypsum and halite between solutions S1 and S5, and solutions S5 and S8; and halite alone between solutions S8 and S10, and S10 and S13. These steps correspond to filtrations 1 to 4. For solutions between S13 and S15, three models are resulted. That of with minimum error is the model of halite, epsomite, and sylvite. This result is in good

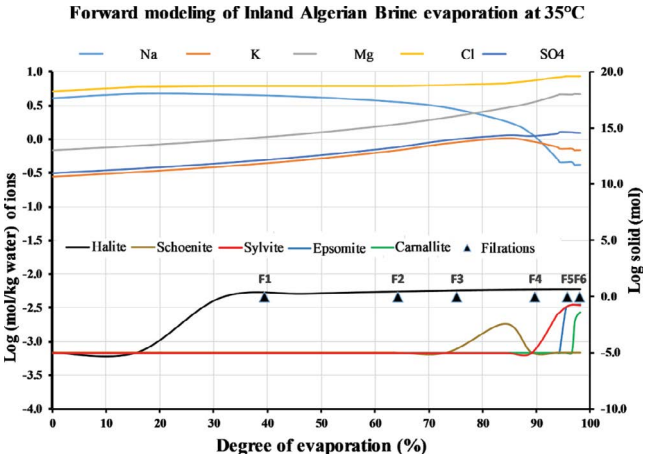

Fig. 8. PHREEQC forward modeled crystallization sequences: F1 + F2 + F3: halite, F4: halite + schoenite, F5: halite + sylvite + epsomite, F6: halite + epsomite + carnallite + sylvite.

agreement with the recovered salt-4. Between solutions S15 and S17, four models returned. The minimum error is that of halite, epsomite, and carnallite. As for salt-5, the sylvite dissolution after appearance of carnallite did not returned because of positive moles transfers. These results corroborate well with the actual crystallization sequences. Indeed, except shoenite, all of the recovered salts by the isothermal evaporation experiment perfectly reproduced by the inverse modeling simulation.

4. Discussion

4.1. Real salts crystallization sequences

The real crystallization sequences given by the identification of the recovered solids S1 to S6, obtained by X-ray diffraction are listed in Table 3. These solids defined five crystallization sequences, salt-1 to salt-5. The first sequence precipitated between density 1.223 to density 1.235, represented by halite and gypsum not predicted by the Jänecke diagram because Ca not included in this system. However, this sequence and the following sequences obtained between densities 1.235 and 1.275 can be assimilated to halite only because of the low amount of gypsum as given in Table 5. Indeed, gypsum disappeared at the density 1.237. These two sequences are in good agreement with the first sequence predicted by the Jänecke diagram that is halite alone. Salt-3 recovered between densities 1.275 and 1.312 is a mixture of halite and schoenite is different from that predicted by Jänecke diagram respected by halite, leonite, and bloedite. It is well known that schoenite replace always leonite because of its faster kinetic and its hexagonal crystallization system favored in supersaturated solutions where the cation $[Mg(H_2O)_6]^2$ prevent the crystallization of no hexagonal salts [30]. Bloedite is a secondary mineral and did not precipitates directly [27]. Salt-4 obtained between filtrations F1 and F5 corresponding to densities from 1.312 to 1.319 is a mixture of halite, epsomite, and sylvite. This sequence is different from that expected by both theoretical and experimental Jänecke diagrams, which is halite,

Table 8
PHREEQC inverse modeling results

Initial solution	Final solution	Solid number	Number of models	Phase mole transfers		Sum of residuals	Sum of delta/ uncertainty limit	Maximum fractional error in element concentration
S1	S5	Solid-1	M1	Gypsum	–0.03	4.87	4.86	0.30
				Halite	–0.80			
			M2	Gypsum	–0.03	5.18	5.17	0.30
S5	S8	Solid-2	M1	Gypsum	–0.01	6.23	6.23	0.50
				Halite	–0.68			
			M2	Gypsum	–0.01	6.65	6.65	0.50
S8	S10	Solid-3	M1	Halite	–0.23	3.45	3.45	0.30
			M2	Nothing		3.82	3.82	0.30
S10	S13	Solid-4	M1	Halite	–0.80	5.02	5.02	0.64
			M2	Nothing		5.56	5.56	0.64
S13	S15	Solid-5	M1	Halite	–0.68	4.14	4.11	0.27
				Schoenite	–0.12			
				Sylvite	–0.07			
			M2	Halite	–0.78	4.32	4.28	0.27
				Schoenite	–0.16			
			M3	Halite	–0.70	5.55	5.47	0.26
				Epsomite	–0.20			
				Sylvite	–0.21			
S15	S17	Solid-6	M1	Halite	–0.81	1.37	1.32	0.43
				Epsomite	–0.68			
				Carnallite	–0.78			
			M2	Halite	–0.71	1.62	1.59	0.48
				Epsomite	–0.59			
				Sylvite	–0.71			
			M3	Halite	–0.68	1.78	1.75	0.49
				Schoenite	–0.28			
				Carnallite	–0.12			
			M4	Halite	–0.68	2.40	2.36	0.49
				Schoenite	–0.34			
			M5	Halite	–0.67	1.92	1.86	0.49
				Schoenite	–0.28			
				Sylvite	–0.12			

bloedite, kainite, hexahydrite and kieserite for the former halite and kainite for the later. Bloedite did not precipitate directly [27] and the slow kinetic of kainite relatively to that of sylvite explains the absence of kainite in the recovered solids. The absence of non-hexagonal salts such as kieserite at highly saturated solutions is well-known and very well documented [26] and references therein. Consequently, epsomite replaced kieserite and hexahydrite. Furthermore, in the solar diagram established by Kurnakov [40], kainite missed and the field of espomite included a large part of that of hexahydrite and kieserite (Fig. 8). Otherwise, this observation corroborates well with the results of [28] where epsomite replace all other magnesium sulfates at relative humidity more than 51%. Contrarily, except the explained replacement of kieserite by epsomite, the following salt precipitated (halite, epsomite, carnallite, and traces of sylvite) between filtrations F5 and F6, corresponding to densities from 1.319 to 1.325, is similar with that (halite, kieserite, and carnallite) of predicted by the forecast and experimental Jänecke diagram. Besides these observations, the projection of the undertaken experimental brine's filtrates on the Kurnakov solar diagram (Fig. 9) reproduced identically the real crystallization sequences from the apparition of epsomite. Schoenite, well identified by X-ray diffraction is the finding and the enigmatic result of this study because it is well-known that it crystalizes in the law temperature (<35°C) and does not occur as primary salt [41]. Schoenite is the result of the complete transformation of kainite, indicating the disappearance of the latter [41]. Moreover, the old diagram of D'ans [42] clearly noticed the presence of the schoenite–kainite paragenesis, and provides the explanation if Autenrieth [43] has not demonstrated, later, in detail, the absence of this paragenesis. According to Braitsch [41], this paragenesis is only possible as a metastable process.

However, the investigation of Susarla and Seshadri [44] when studying equilibria in the system containing chloride and sulfates of potassium and magnesium conclusively established the transition of schoenite and leonite at 32.5°C and higher temperatures. This transition has also clearly shown by the short period of schoenite crystallization in its equilibrium diagram (Fig. 3). This transition has also clearly shown by the short period of schoenite crystallization in its equilibrium diagram (Fig. 3). In addition, schoenite has been associated in stable equilibria with leonite, sylvite, and kainite in the appropriate invariant point of the Jänecke diagram evolving the K^+, Mg^{2+}, Cl^-, $SO_4^{2-}//H_2O$ system at 35°C. This would explain the enigma of the occurrence of schoenite in the salts recovered by the experiment carried out in the present study. Certainly, both forward and inverse PHREEQC modeling with the Pitzer database confirmed the schoenite occurrence with halite and sylvite, and in association with halite alone as returned in the transfer model M1 and M2 between filtrations 4 and 5, respectively (Table 8).

4.2. Theoretical and experimental Jänecke crystallization pathways (crystallization paths and transition lines)

Table 9 presents all of the crystallization sequences obtained by Jänecke solubility diagram, the real recovered salts assemblage, and both PHREEQC forward and inverse modeling. First, after the good agreement of the three first sequences, N°1, N°2 and N°3, a clear deviation is noticed between the two Jänecke pathways, theoretical and experimental. Indeed, the direction of the experimental pathway barely touches the domain of leonite and crosses the line separating the two fields of bloedite and kainite to penetrate directly into the domain of kainite (Fig. 6). The last point of the brine reached the R point. Therefore, the plotted experimental crystallization pathway did not confirm the theoretical forecasted one. Effectively, the first five points of Chott Baghdad natural brine evaporated were inside bloedite crystallization field while the five following points were in the kainite crystallization field, and finally the last point is on the R invariant point (Fig. 6). Consequently, foreseeable sequences 4, 5 and 6 are skipped in the experimental pathway and the experimental sequence N°4 (halite + kainite) was not predicted. This is explained by the study of Autenrieth [45], when modifying the position of invariant points V and R with new determined solubility data. They established that the lines separate the fields of bloedite and kainite, leonite and kainite are not crystallization paths but rather transition lines. Indeed, taking into account solubility data up to the year 1962, Braitsch [41] discussed certain solubility equilibria in the quinary and hexary system with particular importance for the genesis of evaporitic deposits. Thereby, Braitsch pointed out differences of certain minerals associations due to more new investigations since D'ans [46] and van't Hoff [47]. One of this paragenesis was bloedite–kainite at 35°C, which should not exist according to [47] and as reported by Braitsch [41]. This validates intensely the results obtained from Baghdad isothermal evaporation at 35°C where the Jänecke experimental pathway defined the sequence of halite and kainite rather than the sequences 4, 5, and 6 of the theoretical pathway. After Braitsch [41], in this event (transition lines), the composition of the solution changes along the transition line (represented in fine lines in Fig. 10a). The first phase dissolved when the solution has reached a composition, which lies at the intersection of the projection of the line from the salt point of the second phase through the point of the initial solution to the

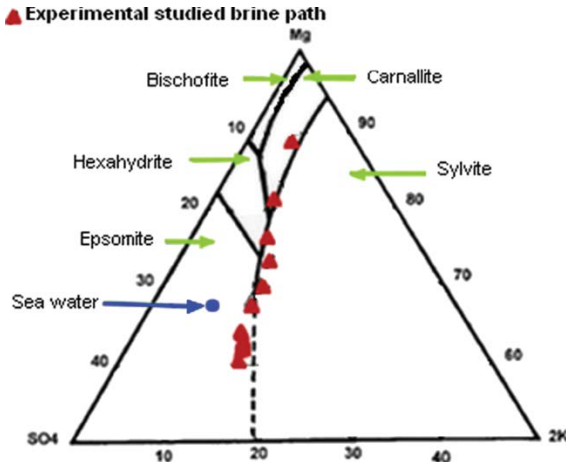

Fig. 9. Projection of Chott Baghdad natural brine (red solid triangles) experimental pathway on the Kurnakov solar diagram.

Table 9
Summary of crystallization sequences obtained by the three approaches

Jänecke solubility diagram		Real (recovered)	PHREEQC modeling	
Predicted	Experimental	Salts	Forward	Inverse
1-Halite	1-Halite	1-Gypsum, Halite	1-Gypsum, Halite	1-Gypsum, Halite
2-Halite, Bloedite	2-Halite, Bloedite	2-Halite	2-Halite	2-Halite
3-Halite, Bloedite, Leonite	3-Halite, Bloedite, Leonite	3-Halite, Schoenite	3-Halite, Schoenite	3-Halite
4-Halite, Bloedite, Kainite 5-Halite, Kainite, Hexahydrite 6-Halite, Kainite, Kieserite	4-Halite, Kainite	4-Halite, Epsomite, Sylvite	4-Halite, Epsomite, Sylvite	4-Halite, Epsomite, Sylvite
7-Halite, Kieserite, Carnallite	5-Halite, Kieserite, Carnallite	5-Halite, Epsomite, Carnallite, Sylvite	5-Halite, Epsomite, Carnallite, Sylvite	5-Halite, Epsomite, Carnallite

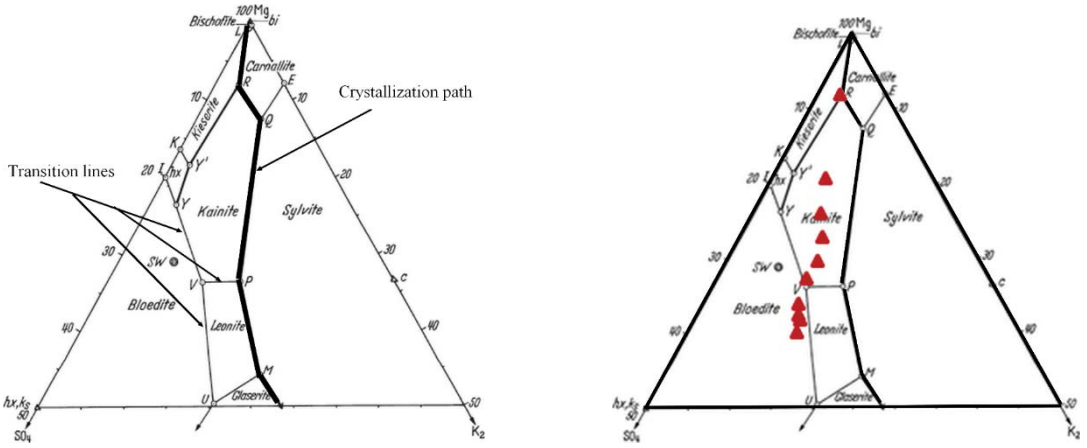

Fig. 10. (a) 35° isotherm of the five-component system saturated in NaCl, Mg corner, stable equilibria. Crystallization paths heavy lines, fine lines are transition lines. Points V-R calculated from new data of Autenrieth and Braune, in Braitsch [41]. (b) Projection of studied brine pathway on the new Autenrieth and Braune modified quinary diagram for 35°C isotherm.

transition line. There, more of the second solid phase precipitates and the composition of the solution moves into the stability field of the second phase (kainite, in our case). On the other hand, along the crystallization paths (shown as heavy lines in Fig. 9), the two adjacent solid phases can, both, precipitate simultaneously, with the composition of the solution changing along the boundary curve to a corner point. The geometric significance of this is that in such a figure the boundary lines between stability fields in isothermal figures must be linear [41]. These results are obtained when plotting the experimental pathway of the undertaken brine on the modified quinary diagram after Autenrieth and Braune (Fig. 10b), which shows that the experimental pathway did not overlap the transition lines (fines lines) but cross them, rather parallel to the crystallization paths (solid lines). For this reason, theoretical sequences 4 (halite + bloedite + kainite), 5 (halite + kainite + hexahydrite), and 6 (halite + kainite + kieserite) are absent in the experimental pathway and replaced by only the alone sequence 4 which is halite + kainite. The last sequence (halite + kieserite + carnallite) is identic for both theoretical and experimental pathways because the brine left the kainite field. This observation confirmed that not all lines in the Jänecke diagram are crystallization paths, and contribute to understand the crystallization of sylvite, which is outside of the Jänecke experimental pathway. This is due to its faster kinetic crystallization than that of kainite.

4.3. PHREEQC forward and inverse modeling

As for Jänecke diagram, the forward modeling does not concern the first sequence. It intentionally ignored Ca in order to prevent the back reaction of calcium-bearing minerals. This assumption is plausible as Ca-bearing phases were removed from the solution in the earlier stages of evaporation. All other sequences obtained by the forward modeling are in very good agreement with the recovered salts. Table 8 shows clearly this agreement. The inverse modeling performed on the real ionic composition of the evaporated brine at each two successive filtrations returned one or more models of minerals associations translated by negative phase transfers. Those with minimum residual error are strongly similar with the recovered solids (Table 7). Indeed, except the absence of schoenite in the third inverse modeling sequence, all of others salts are returned by the inverse simulation. This confirms that Pitzer thermodynamic database is a powerful tool to the study of the concentrated brines [27,39,48,49].

5. Conclusion

This study reports the results of Chott Baghdad natural brine evolution during the isothermal evaporation experiment at 35°C. The evolution of density and ionic composition of the studied brine studied with several tools. A materiel balance was then, calculated based on the experimental evolution of the brine. The Jänecke projection of quinary solubility diagram Na^+, K^+, Mg^{2+}, Cl^-, $SO_4^{2-}//H_2O$ was used to predict the theoretical and the experimental crystallization pathways. Finally, this isotherm evaporation experiment has been simulated using PHREEQC with the Pitzer thermodynamic database. The conclusions are:

- The real crystallization sequences obtained by X-ray diffraction on the recovered solids are 1st) gypsum + halite, 2nd) halite + schoenite, 3rd) halite + epsomite + sylvite and finally 4th) halite + epsomite + sylvite + carnallite. These salts conclusively confirmed with equilibrium diagrams of the sampled brines.
- The calculated materiel balance proves that Chott Baghdad natural brine is very rich in potassium and magnesium salts, in addition to halite. Definitely, the calculations performed for a quantity of the brine containing 1,000 moles of water indicate that after evaporation 90% of water, the mass percentages of recovered salts are 71.21% of NaCl, 17.77% of $MgSO_4$ and 9.84% for KCl. Thus, more than a quarter of the salts recovered mass consists of potassium chloride and magnesium sulfate. Furthermore, the total mass of solids calculated for 1,000 moles with this method is 7,683.5 g. This later

related to the amount of brine used in the experiment is 1,707.33 g. The actual mass of solids recovered is 1,718 g. The difference is 0.6%. Thus, the calculated balance sheet is satisfactory.

- The deviation between the theoretical and the experimental crystallization pathways confirmed the fact that not all lines in Jänecke diagram are crystallization path. As found by Autenrieth and Braune and reported by Braitsch [41], the same paragenesis (halite + kainite) was obtained by the experimental results of the Baghdad brine. The experimental pathway cross the transitional lines and penetrates under the crystallization field of kainite. Thus, the clear difference observed between the theoretical and the experimental pathway explained by the fact that the surfaces limiting kainite, bloedite and leonite fields are note crystallization pathways but transition lines as established by Autenrieth and Braune and reported by Braitsch [41] in page 74. This result, rarely obtained, may be considered as a finding.
- The Jänecke crystallization pathways are different from the real crystallization sequences characterized by X-ray powder diffraction of the recovered salts. The difference is the absence of bloedite, leonite, kainite, hexahydrite, and kieserite in the recovered salts. In the other hand, the occurrence of schoenite in the recovered solids. The Kurnakov solar diagram explains the absence of bloedite, leonite, hexahydrite, and kieserite where these salts are missed. This is due to the apparition of the complex cation $[Mg(H_2O)_6]^{2+}$, which disfavors the crystallization of a non-hexagonal crystalline system minerals (i.e., kainite) [26,30]. Indeed, at this advanced stage of evaporation minerals that do not have an octahedral crystalline form like kainite and bloedite do not crystallize [30,31]. Thus, epsomite replaced all of these salts in this experiment.
- The enigmatic finding of this work is the occurrence of schoenite well identified by X-ray diffraction on the solids recovered in the fourth filtration. Because it is known that schoenite crystallizes at low temperatures (<35°) and does not exist on the 35°C quinary solubility diagram. However, the old diagram of D'ans [42] which clearly noticed the presence of the schoenite–kainite paragenesis provides the explanation although Autenrieth [43] has demonstrated in detail the absence of this paragenesis. According to Braitsch [44], this paragenesis is only possible as a metastable process. However, the more recent investigation established the transition of schoenite and leonite at 32.5°C and higher temperatures where schoenite has been associated in stable equilibria with leonite, sylvite, and kainite in the K^+, Mg^{2+}, Cl^-, SO_4^{2-}// H_2O system at 35°C. This would explain the enigma of the occurrence of schoenite in the salts recovered by the experiment carried out in the present study. On the other hand, both forward and inverse PHREEQC modeling with the Pitzer database confirmed the schoenite occurrence, with halite (alone) and with halite and sylvite, respectively, in the transfer models M1 and M2 of the fifth solid (solid-5). This corroborates very well with the result obtained by this study where occurrence of shoenite, as showed by the equilibrium diagram of brines, has been brief and crystallized only between B11 and B12-S4.
- The projection of the experimental results of Chott Baghdad brine on the Kurnakov solar diagram showed a very good agreement after the epsomite apparition. This diagram is a powerful tool to predict the evolution of brine evaporation. Especially to very documented like-marine brine type because many studies concerned seawater evolution.
- The PHREEQC modeling of the isothermal evaporation experiment successfully returned the observed results. This confirms that the PHREEQC code is a powerful tool for studying the evaporation processes of supersaturated brines.
- Finally, Chott Baghdad brine reminds the case of marine-like potash evaporate formation on a continental playa of Chott el Djerid, southern Tunisia studied by Bryant et al. [50]. Thus, the inland Chott Baghdad brine seems to be a marine-like water.

References

[1] M. Zatout, R.L. López Steinmetz, M. Hacini, S.B. Fong, A. M'nif, A.H. Hamzaoui, L.C. López Steinmetz, Saharan lithium: brine chemistry of chotts from eastern Algeria, Appl. Geochem., 115 (2020) 104566, doi: 10.1016/j.apgeochem.2020.104566.
[2] A. Guendouz, A.S. Moulla, W.M. Edmunds, K. Zouari, P. Shand, A. Mamou, Hydrogeochemical and isotopic evolution of water in the Complexe Terminal aquifer in the Algerian Sahara, Hydrogeol. J., 11 (2003) 483–495.
[3] M.S.M. Abdel Wahed, E.A. Mohamed, M.I. El-Sayed, A. M'nif, M. Sillanpää, Crystallization sequence during evaporation of a high concentrated brine involving the system Na–K–Mg–Cl–SO_4-H_2O, Desalination, 355 (2015) 11–21.
[4] C. Djebali, L. Zayani, A. M'nif, R. Rokbani, Etude sur la réactivation des saumures naturelles du sud tunisien, J. Soc. Chim. Tunis., 4 (1998) 233–244.
[5] M. Zatout, Geochemistry and Mining Potential of Lithium in the Southern Algerian Chotts: Basin of Ouargla, Melghir and Merouane, Dissertation, Kasdi Merbah University, Ouargla, Algeria, 2017, 168 p.
[6] M. Bąbel, B. Charlotte Schreiber, Chapter 9.18 – Geochemistry of Evaporites and Evolution of Seawater, M. Fred, Ed., Treatise on Geochemistry, 2nd ed., Vol. 9, Sediments, Diagenesis, and Sedimentary Rocks, Elsevier, Oxford, 2014, pp. 483–560, doi: 10.1016/B978-0-08-095975-7.00718-X.
[7] C. Funk, S. Shukla, Chapter 7 – Theory—Understanding Atmospheric Demand in a Warming World, C. Funk, S. Shukla, Eds., Drought Early Warning and Forecasting, Elsevier, Amsterdam, Netherlands, 2020, pp. 101–115, doi: 10.1016/B978-0-12-814011-6.00007-5.
[8] A. Katz, A. Starinsky, Geochemical history of the Dead Sea, Aquat. Geochem., 15 (2009) 159–194.
[9] A.M. Salhotra, E. Eric Adams, D.R.F. Harleman, Effect of salinity and ionic composition on evaporation: analysis of dead sea evaporation pans, Water Resour. Res., 21 (1985) 1336–1344.
[10] C.E. Harvie, J.H. Weare, The prediction of mineral solubilities in natural waters: the Na-K-Mg-Ca-Cl-SO_4//H_2O system from zero to high concentration at 25°C, Geochim. Cosmochim. Acta, 44 (1984) 981–997.
[11] C.E. Harvie, N. Møller, J.H. Weare, The prediction of mineral solubilities in natural waters: the Na-K-Mg-Ca-H-Cl-SO_4-OH-HCO_3-CO_3-CO_2-H_2O system to high ionic strengths at 25°C, Geochim. Cosmochim. Acta, 48 (1984) 723–751.
[12] I. Grenthe, A. Plyasunov, On the use of semiempirical electrolyte theories for modeling of solution chemical data, Pure Appl. Chem., 69 (1997) 951–958.
[13] C. Ye, J. Mao, Y. Ren, Y. Li, Y. Lin, I.M. Power, Y. Luo, Salt crystallization sequences of nonmarine brine and their application for the formation of potassium deposits, Aquat. Geochem., 24 (2018) 209–229.

[14] M.A. McCaffrey, B. Lazar, H.D. Holland, The evaporation path of seawater and the coprecipitation of Br^- and K^+ with halite, J. Sediment. Petrol., 57 (1987) 928–938.
[15] D.M. Deocampo, B.F. Jones, Chapter 7.13 – Geochemistry of Saline Lakes, H.D. Holland, K.K. Turekian, Eds., Treatise on Geochemistry, Vol. 7, Surface and Groundwater, Weathering, and Soils, 2nd ed., Elsevier, Oxford, 2014, pp. 437–469, doi: 10.1016/B978-0-08-095975-7.00515-5.
[16] A. Haddane, M. Hacini, A. Bellaoueur, A.H. Hamzaoui, A. M'Nif, Effect of evaporite paleo-lacustrine facies on the brines geochemistry, economy implication. Case of chott Bagdad El Hadjira Ouargla, South-Eastern Algeria, Energy Procedia, 119 (2017) 228–235.
[17] A. Lamini, Minéralogie des chotts de la région d'El Hadjira, Kasdi Merbah Ouargla, 2012.
[18] A. Lamini, M. Hacini, Geology and geochemistry of endoroique basin case of Baghdad chott southern of Algeria, AIP Conf. Proc., 1968 (2018), doi: 10.1063/1.5039165.
[19] M. Zatout, M. Hacini, A. Lamini, S.B. Fong, A.H. Hamzaoui, A. M'nif, M.S.M. Abdel Wahed, Geochemical characterization of the Southern Algerian brines using PHREEQC software and the Jänecke solubility phase diagram, Arabian J. Geosci., 15 (2022) 1247, doi: 10.1007/s12517-022-10441-7.
[20] M. Zatout, M. Hacini, A.H. Hamzaoui, A. M'nif, Sequence crystallization during isotherm evaporation of southern Algeria Chott Baghdad natural brine, J. Fundam. Appl. Sci., 9 (2017) 959, doi: 10.4314/jfas.v9i2.22.
[21] Z. Janecke, Erganzung zu der neuen Darstellungsform der van't Hoffschen Untersuchungen (Complement to the new form of the van't Hoff's investigations), Anorg. Allgem. Chem., 53 (1907) 319.
[22] H. Hammi, J. Musso, A. M'nif, R. Rokbani, Tunisian salt lakes evaporation studied by the DPAO method based on solubility phase diagrams, Desalination, 158 (2003) 215-220.
[23] H. Hammi, A. M'nif, R. Rokbani, Étude de l'évaporation d'une saumure naturelle. Corrélation conductivité-concentrations ioniques (Na^+, K^+, Mg^{2+}, Cl^-, SO_4^{2}), J. Phys. IV France, 11 (2001) Pr10-63 – Pr10-70, doi: 10.1051/jp4:20011008.
[24] S. Attia-Essaies, L. Zayani, D. Ben Hassen Chehimi, R. Cohen Adad, N. Kbir Ariguib, M. Trabelsi-Ayadi, Simulation of crystallization sequence during the evaporation of Chott El Jerid brine (south Tunisia), Thermochim. Acta, 503–504 (2010) 8–11.
[25] F. Khlissa, A. M'nif, R. Solimando, R. Rokbani, Prediction of mineral precipitation during isotherm evaporation of southern Tunisian natural brines, Desalination, 166 (2004) 261–266.
[26] A. M'nif, R. Rokbani, Minerals successions crystallisation related to Tunisian natural brines, Cryst. Res. Technol., 39 (2004) 40–49.
[27] W. Voigt, What we know and still not know about oceanic salts, Pure Appl. Chem., 87 (2015) 1099–1126.
[28] D. Benavente, P. Brimblecombe, C.M. Grossi, Thermodynamic calculations for the salt crystallisation damage in porous built heritage using PHREEQC, Environ. Earth Sci., 74 (2015) 2297–2313.
[29] S. Attia Essaies, L. Zayani, D. Ben, D.B.H. Chehimi, M. Trabelsi Ayadi, An Indian Journal, Study of the evaporation of Tunisian brine (Chott El Jerid) comparison between the sequences of crystallization experimental and theoretical, Mater. Sci., 9 (2013) 367–371.
[30] Chr. Balarew, Solubilities in seawater-type systems: some technical and environmental friendly applications, Pure Appl. Chem., 65 (1993) 213–218.
[31] M. Smith, J.S. Compton, Origin and evolution of major salts in the Darling pans, Western Cape, South Africa, Appl. Geochem., 19 (2004) 645–664.
[32] R. Barzegar, A. Asghari Moghaddam, A.H. Nazemi, J. Adamowski, Evidence for the occurrence of hydrogeochemical processes in the groundwater of Khoy plain, northwestern Iran, using ionic ratios and geochemical modeling, Environ. Earth Sci., 77 (2018) 597, doi: 10.1007/s12665-018-7782-y.
[33] D.L. Parkhurst, C.A.J. Appelo, Description of Input and Examples for PHREEQC Version 3—A Computer Program for Speciation, Batch-Reaction, One-Dimensional Transport, and Inverse Geochemical Calculations, U.S. Geological Survey, Denver, Colorado, 2013. Available at: https://doi.org/10.1097/00000446-195210000-00005
[34] Y. Rafighdoust, Y. Eckstein, R.M. Harami, M.H.M. Gharaie, A. Mahboubi, Using inverse modeling and hierarchical cluster analysis for hydrochemical characterization of springs and Talkhab River in Tang-Bijar oilfield, Iran, Arabian J. Geosci., 9 (2016) 241, doi: 10.1007/s12517-015-2129-4.
[35] K.S. Pitzer, Thermodynamics of electrolytes. I. Theoretical basis and general equations, J. Phys. Chem., 77 (1973) 268–277.
[36] I.K. Zherebtsova, N.N. Volkova, Experimental study of behavior of trace elements in the process of natural solar evaporation of Black Sea water and Sasyk–Sivash brine, Geochem. Int., 7 (1966) 656–670.
[37] L. Zayani, R. Rokbani, Crystallisation of oceanic salts, J. Therm. Anal. Calorim., 57 (1999) 575–585.
[38] I. Prigogine, R. Defay, Thermodynamique Chimique, Éditions Desoer, Dunod, Liège, Paris, 1950.
[39] P. Lu, G. Zhang, J. Apps, C. Zhu, Comparison of thermodynamic data files for PHREEQC, Earth Sci. Rev., 225 (2022) 103888, doi: 10.1016/j.earscirev.2021.103888.
[40] N.S. Kurnakov, V.I. Nikolaev, Izv. Sekt. Fiz. Khim. Anal. 10, 333 (1938), N.S. Kurn, Moscow, 1963.
[41] O. Braitsch, The Stability Conditions of Salt Minerals, in: Salt Deposits Their Origin and Composition. Minerals, Rocks and Inorganic Materials, Vol. 4, Springer, Berlin, Heidelberg, 1971, pp. 27–83. Available at: https://doi.org/10.1007/978-3-642-65083-3_2
[42] J. D'ans, The Solution Equilibria of Systems of Salts of Oceanic Salt Deposits, VerI. Ges., 254 S. Potash Research Institute, Berlin, 1933.
[43] H. Autenrieth, New Studies on the Quinary NaCl-Saturated System of Salts of Oceanic Saiz Deposits Important for Potash Crude Ore Processing, Kali u.Steinsalz. 1, H. (1955) 18–32.
[44] V.R.K.S. Susarla, K. Seshadri, Equilibria in the system containing chloride and sulphates of potassium and magnesium, Proc. Indian Acad. Sci. - Chem. Sci., 91 (1982) 315–320.
[45] H. Autenrieth, The stable and metastable equilibria of the reciprocal salt pair $K_2Cl_2 + MgSO_4 + K_2SO_4 + MgCl_2$ without and with NaCl as the soil body, and their application in practice, Kali u. Steinsalz. 1, H. (1954) 3–22.
[46] J. D'ans, Untersuchungen iiber die Salzsysteme ozeanischer Salzablagerungen, Exp. Bearbeitet Mit A. Bertsch Und A. Gessner. Kali., 9 (1915).
[47] J.H. Van't Hoff, Sitzung vom 9. October 1905, 38, Ber. Dtsch. Chem. Ges., 38 (1905) 3211–3216.
[48] R. Slimani, A. Guendouz, F. Trolard, A.-S. Moulla, B. Hamdi-Aïssa, G. Bourrié, Geochemical inverse modeling of chemical and isotopic data from groundwaters in Sahara (Ouargla basin, Algeria), Hydrol. Earth Syst. Sci. Discuss., (2016) 1–49.
[49] D.L. Parkhurst, A. Tony, User's Guide to PHREEQC Version 3 - A Computer Program for Speciation, Batch-Reaction, One-Dimensional Transport, and Inverse Geochemical Calculations, Colorado, 1999.
[50] R.G. Bryant, B.W. Sellwood, A.C. Millington, N.A. Drake, Marine-like potash evaporite formation on a continental playa: case study from Chott el Djerid, southern Tunisia, Sediment. Geol., 90 (1994) 269–291.